Article

Hydrogel-Based Bioinks for Cell Electrowriting of Well-Organized Living Structures with Micrometer-Scale Resolution

Miguel Castilho,*,[⊥] Riccardo Levato,[⊥] Paulina Nunez Bernal, Mylène de Ruijter, Christina Y. Sheng, Joost van Duijn, Susanna Piluso, Keita Ito, and Jos Malda

Read Online

ACCESS | Metrics & More | Article Recommendations | Supporting Information

ABSTRACT: Bioprinting has become an important tool for fabricating regenerative implants and *in vitro* cell culture platforms. However, until today, extrusion-based bioprinting processes are limited to resolutions of hundreds of micrometers, which hamper the reproduction of intrinsic functions and morphologies of living tissues. This study describes novel hydrogel-based bioinks for cell electrowriting (CEW) of well-organized cell-laden fiber structures with diameters ranging from 5 to 40 μm. Two novel photo-responsive hydrogel bioinks, that is, based on gelatin and silk fibroin, which display distinctly different gelation chemistries, are introduced. The rapid photomediated cross-linking mechanisms, electrical conductivity, and viscosity of these two engineered bioinks allow the fabrication of 3D ordered fiber constructs with small pores (down to 100 μm) with different geometries (*e.g.*, squares, hexagons, and curved patterns) of relevant thicknesses (up to 200 μm). Importantly, the biocompatibility of the gelatin- and silk fibroin-based bioinks enables the fabrication of cell-laden constructs, while maintaining high cell viability post printing. Taken together, CEW and the two hydrogel bioinks open up fascinating opportunities to manufacture microstructured constructs for applications in regenerative medicine and *in vitro* models that can better resemble cellular microenvironments.
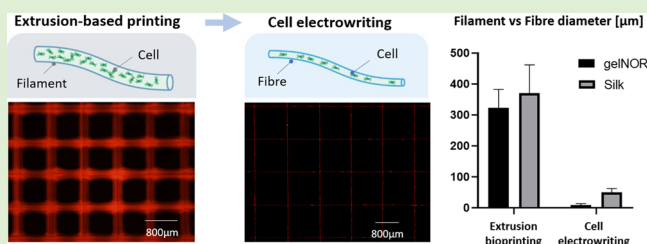
INTRODUCTION

Bioprinting is an emerging technique for the fabrication of biological constructs that can be used in regenerative medicine (RM) and *in vitro* drug testing.[1] However, in an attempt to better mimic native tissues, there is an increasing demand to engineer structures with finer resolutions and further capture the hierarchical structure and composition of the native extracellular matrix.[2,3] This mimicking of the cellular microenvironment could provide new opportunities for the generation of constructs that can successfully exhibit functions at tissue and organ levels.[4−6] For example, intercellular interactions at the micro- to nanometer scale,[7] spatiotemporal changes in the ECM structure,[8,9] and mechanical and topographical cues provided by fibrillar ECM components are the well-known key drivers of cell behavior[10−12] and are the likely crucial elements for the engineering of functional, tissue-like constructs. Until today, the most well-established bioprinting processes, namely, extrusion-based,[13,14] droplet-based,[15] and light-assisted,[16] with the notable exception of two-photon polymerization,[17] are limited to resolutions close to tens of micrometers, which hamper the reproduction of such cellular microenvironments.

Recently, attempts have been made to achieve high-resolution biological constructs by using biofabrication processes, such as electrospinning[18−20] and electrohydrodynamic jetting.[21,22] In both methods, and differently from the conventional extrusion bioprinting techniques, material flow is driven by electrical forces that surpass the surface tension of the liquid ink, allowing for the fabrication of fibers with sizes smaller than the extrusion nozzle diameter.[23] Despite the high-intensity electrical field involved, these methods were found to be compatible with the processing of living cells, even showing initial steps toward the reconstruction of hierarchical structures embedding cardiomyocytes,[18] or cells from neural lineage.[24] Nevertheless, neither of these techniques could simultaneously meet the requirements to emulate the intrinsic morphologies and local composition of cellular microenvironments, that is, the three-dimensional (3D) patterning, the deposition of fibers with micron/submicron size diameters, and the maintenance of high cell viability. Despite the fact that electrospinning approaches are compatible with the generation of cell-laden microfibers, they could not be readily applied to organize the fibers into predefined 3D shapes because of the whipping instabilities of the electrified jet.[18,25] With electrohydrodynamic jetting, on the other hand, structures with more complex
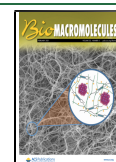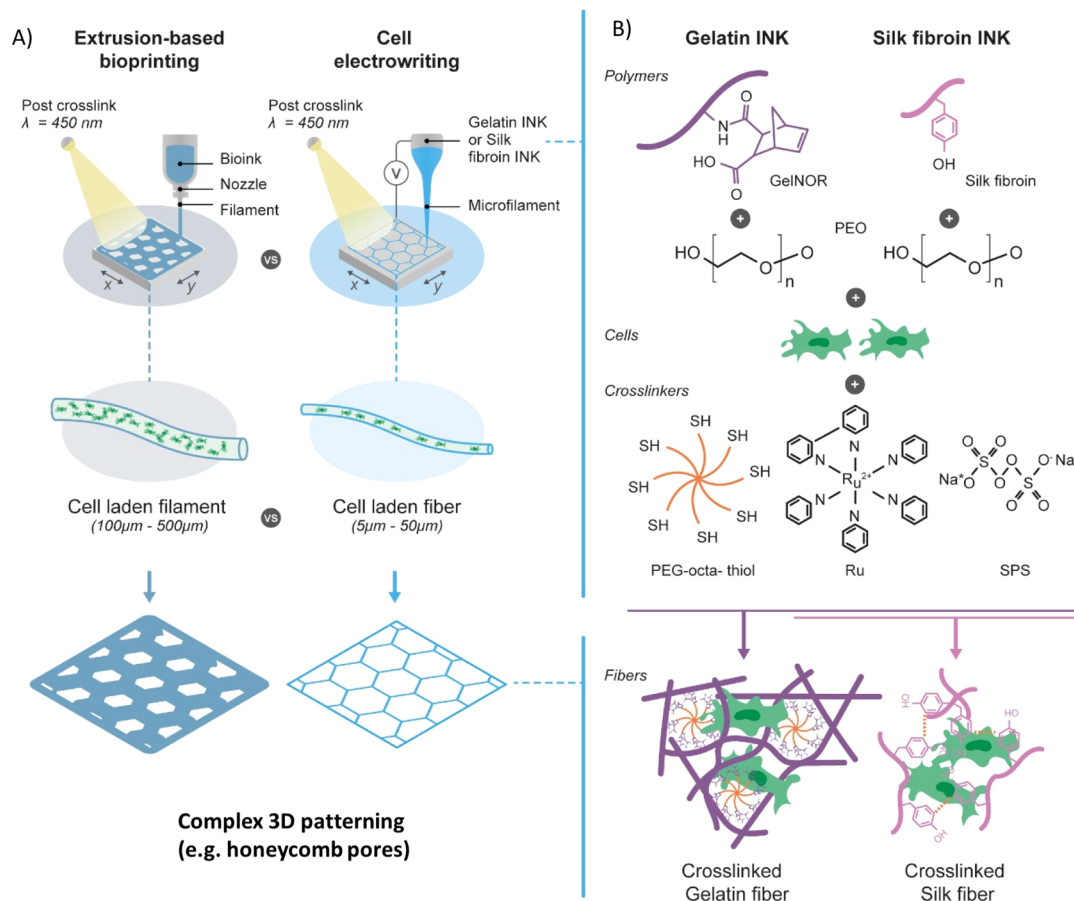
Figure 1. (A) Comparison between conventional extrusion-based bioprinting and novel CEW process with respective differences in cell distribution and process resolution. (B) Schematic of the developed gelatin and silk fibroin bioink compositions with their respective light photo-cross-linking mechanism. Scheme illustrates the visible light-initiated orthogonal cross-linking of (i) gelnor with a PEG thiol cross-linker and (ii) silk fibroin, in the presence of ruthenium and SPS. Gelnor and silk bioinks are compatible with both extrusion-based printing and CEW.

3D patterns could be created, yet fabrication resolution was compromised.[21,26,27] In addition, most of the previous studies on nonthermal electrohydrodynamic jetting have been carried out with polysaccharide-based hydrogels, such as alginate, which present poor cell adhesive properties and limited mechanical toughness.[21,28] Thermal electrohydrodynamic jetting, on the other hand, has mostly been based on the use of synthetic polymers, such as poly(2-ethyl-2-oxazine) and ureido-pyrimidinone coupled to poly(ethylene glycol),[22,27,29−31] which are not compatible with cell encapsulation. In particular, melt Electrowriting (MEW) is a technique that has gained increased attention in RM because of its potential to engineer highly ordered fibrous scaffolds but until now is still limited to the use of biomaterial inks, that is, thermoplasts and hydrogel-based materials, without encapsulated cells, because of the high processing temperatures required. Table S1 in the Supporting Information summarizes the material platform, resolution, shape control, and cell encapsulation capabilities of previously reported electrohydrodynamic fabrication technologies.

There is a clear need for the development of biomaterial platforms that are compatible with processing through the application of strong electrical fields, allow for the fabrication of complex small-scale geometries, and support high viability of encapsulated cells. Protein-based natural-derived materials are promising candidates because of their inherent biocompatibility, bioactive signals, binding affinity for cells, and tunable

mechanical properties. Here, we describe a new class of photo-cross-linkable bioinks based on proteinaceous polymers, namely, gelatin and silk fibroin, that are compatible with the abovementioned requirements and thus can enable the 3D writing of microscale, cell-laden fibers *via* a cell electrowriting process (CEW) (Figure 1). This process conjoins the principles of electrical-assisted material deposition with cell-laden hydrogel extrusion, moving beyond the existent nozzle-based bioprinting processes and MEW technology. We selected gelatin, as it is derived from collagen, the main organic constituent of the natural ECM of mammals,[32] and silk fibroin because of its unique mechanical properties and potential for cell encapsulation.[33,34] These protein-based polymers with complementary biological and mechanical properties could aid in further approaching the functional and structural properties of native cellular microenvironments, while additionally demonstrating the flexibility in material processing of the CEW for biofabrication.

■ EXPERIMENTAL SECTION

Materials. The following materials were used: gelatin type A (bloom 180, Roth, Germany); 8-arm poly(ethylene glycol) thiol (MW: 10,000 g/mol; JenKem Technology, USA); tris(2,2′-bipyridyl)dichlororuthenium(II) hexahydrate (Ru; Sigma-Aldrich, The Netherlands); sodium persulfate (SPS; Sigma-Aldrich, The Netherlands); poly(ethylene oxide) (PEO; MW: 600,000−1,000,000 g/mol, Acros Organics, USA); silkworm cocoons (Wild Fibres, UK); and lithium bromide (Acros Organics, USA).

Gelnor Preparation. Gelnor was synthesized as previously described.[35] Briefly, 10% (w/v) porcine gelatin type A (180 bloom; Roth, Germany) was dissolved in phosphate-buffered saline (PBS) at 50 °C under constant stirring conditions. A 20% (w/v) of carbic anhydride (CA; Acros Organics, Japan) was added to the gelatin solution, and the pH was adjusted to 7.5−8.0 using 5 M sodium hydroxide (NaOH). The reaction was quenched after 24 h by the addition of 3× PBS. After centrifugation at 4000 rpm to remove excess CA, gelnor was dialyzed against deionized water (Milli-Q) at 5 °C for 5 days, and water was refreshed 2× per day. Finally, the solution was filter-sterilized and lyophilized. The degree of functionalization was 45%, as determined by fluoraldehyde assay, as previously reported.[35]

Silk Fibroin Preparation. Silk fibroin was extracted from *Bombyx mori* silkworm cocoons, as previously described.[34] Briefly, cut cocoons were boiled in an aqueous solution of 0.02 M Na_2CO_3 for 30 min. The degummed fibers were dissolved in a 9.3 M LiBr (Sigma-Aldrich) solution at 70 °C for 1 h, followed by dialysis against water for 48 h, using cellulose dialyzing tubing (MWCO 3.5 kDa, Sigma-Aldrich). The resulting 6% (w/v) silk solution was concentrated to 16% (w/v) by dialysis against PEG (10 kDa, Sigma-Aldrich).

Bioink Preparation. Stock gelnor solutions were mixed with solutions having different PEO concentrations to obtain a blend with the final gelnor concentration of 10% and various PEO contents (1−6% w/v). A 10% (w/v) PEO stock solution was prepared by dissolving PEO powder in Milli-Q water. The gelnor/PEO blends were gently mixed at room temperature, followed by the addition of Ru and SPS at various ratios (2:5, 2:10, and 2:20). Concentrated silk solutions were prepared with the PEO concentrations same as the gelnor ink. The silk fibroin/PEO blend was mixed at 4 °C, followed by the addition of Ru and SPS at the same ratios as that of gelnor.

Rheological Measurements. Rheological characterizations of gelnor, gelnor/PEO, silk, and silk/PEO were performed on a rheometer (Discovery HR-2, TA instruments) fitted with a parallel plate of 20 mm in diameter, a gap distance of 0.5 mm, and equipped with a light-curing system. To determine the gelation time, the bioink solutions with different Ru/SPS ratios were placed between the two plates. *In situ* photorheometry was performed by using a visible light source, with light switched on 30 s after initiating the time sweep measurement. All measurements were performed within the linear viscoelastic region, at a strain of 1% and room temperature. The elastic modulus (G') and viscous modulus (G'') were recorded as functions of time. To determine viscosity as a function of shear rate, the bioink solutions were placed between the parallel plates, and data were collected over a shear rate range between 1 and 1000 s^{-1}. The photorheometry and hydrogel cross-linking experiments were conducted using a 600 lumen white lamp, with the wavelength range of 400−700 nm.

Electrical Conductivity. The conductivity of the different hydrogel compositions was evaluated using a CDM230 conductivity meter (Radiometer Analytical, France). Calibration was first conducted using NaCl solutions (0.1 and 1% w/v).

Sol Fraction Analysis. Cross-linking efficiency was assessed through sol fraction analysis, as previously reported in the literature.[36] First, cylindrical gels (Ø = 6 mm × h = 2 mm) were prepared in custom-made Teflon molds and cross-linked by exposure to visible light irradiation (wavelength 400−450 nm) for 45 s. All cross-linked cylinders were weighted for their initial weight ($m_{in\ t=0}$) and three lyophilized samples to obtain dry weights ($m_{dry\ t=0}$). The remaining samples were incubated in PBS at 37 °C, freeze-dried, and weighted again (m_{dry}). The sol fraction was then determined as follows: sol fraction = $((m_{in\ t=0} - m_{dry})/m_{in\ t=0})$.

FTIR spectra. Infrared (IR) spectra were obtained on a FTIR spectrometer (PerkinElmer Spectrum Two, with a universal ATR sampling accessory and equipped with a diamond crystal, PerkinElmer Instruments, The Netherlands). The IR spectra were measured at room temperature in reflection mode, with the wavelength region from 4000 to 450 cm^{-1}. Gelnor and silk-based CEW bioinks before and after incubation in PBS for 0, 24, and 72 h were analyzed. All samples were freeze-dried for 24 h before analysis. The FTIR spectra

were processed for peak deconvolution, integration, and analysis with the OriginPro 8 software package (Origin Lab, USA). Upon identification of the key characteristic peaks of the macromolecules present in the hydrogel formulations, the area under the peaks was calculated. The presence of residual PEO within the hydrogels was estimated by calculating the ratio of the area under the peaks representing the asymmetric C−O−C stretch at 1090 cm^{-1} (characteristic of the ether bonds in PEO) and the amide I band (characteristic of protein compounds like gelatin and silk).

Cell Electrowriting. Hydrogel fabrication was performed with an in-house-built device (Figure S6). Briefly, the hydrogel was loaded in a temperature-controlled printhead (temperature range 0−120 °C) connected to a high-precision air pressure (0.01−2 bar, VPPE-3-1-1/8-2-010-E1 557771, Festo). The hydrogel was electrified with a high-voltage power supply (Heinzinger LNC 30000-2pos, 0−30 kV), and the electrified hydrogel fiber was collected in a computer-controlled high-precision XYZ stage (LG-motion, UK). The CEW device was protected by an acrylic box to ensure stable environmental conditions. All the fabrication experiments were performed at room temperature using glass syringes (3 mL, 25 G needle nozzle). Hydrogel jet formation as well as fiber diameter and morphology were investigated at an increasing voltage of [2, 5] kV, for a constant velocity of 25 mm/s and pressure of 0.05 bar; at an increasing collection velocity of [5, 50] mm/s, for constant voltages of 2.5 kV (gelnor) and 3 kV (silk) and pressure of 0.05 bar; and at an increasing pressure of [0.05, 0.3] bar, for a constant collection velocity of 25 mm/s and voltages of 2.5 kV (gelnor) and 3.0 kV (silk). Print fidelity and layer stacking experiments were performed at a constant collector velocity of [25, 30] mm/s, voltages of 2.5 (gelnor) and 3.0 (silk), and air pressure of 0.05 bar. All experiments were conducted at a constant collector distance of 5 mm, and the constructs were irradiated with visible light (400−450 nm) during jet collection and after printing for approx. 5 min. Square- and hexagon-shaped pore fabrication experiments were performed with the same CEW parameters. Jet and scaffold fabrications were monitored by digital USB microscopes.

Extrusion-Based Bioprinting. Extrusion printing of gelnor and silk hydrogels was achieved by pneumatic dispensing with a CELLINK INKREDIBLE bioprinter (CELLINK, Sweden). Extrusion was performed at room temperature, with a 25 G needle tip, collector velocity of 10 mm/s, and an applied pressure of 0.9 bar. After printing, the constructs were irradiated with visible light (400−450 nm) for approx. 5 min.

Swelling and Mechanical Evaluation. Swelling was evaluated by first immersiing CEW fibers in PBS over 14 days, followed by imaging the fibers before and after 1 h, 1, , 2, 3, 7, and 14 days of immersion by fluorescence microscopy. The fiber diametral changes were measured at each time point. For simplicity, the fibers were assumed to expand in an isotropic manner. The mechanical behavior of the gelnor and silk-based scaffolds obtained by CEW and extrusion-based printing was assessed by a displacement-controlled Piuma nanoindenter (Optics 11, The Netherlands). A probe with a spherical indenter tip with a radius of 28 μm and a stiffness of 0.51 N/m was used. Probe displacement was set to 10% of the specimen thickness. The effective elastic modulus (stiffness) was derived by fitting the load−displacement curves to the Hertzian contact model, between 0 and 30% of the maximum load point. At least five scaffolds of each composition and fabrication process were tested.

Fiber and Scaffold Imaging. An Olympus BX51 fluorescent microscope (Olympus, The Netherlands) was used with a TRITC filter to obtain high-magnification images of the printed hydrogel fibers. Fluorescence microscopy for fiber quality analysis was performed through imaging the natural fluorescence exhibited by gelatin and silk polymers. Stereomicroscopy images of the fabricated 3D constructs were acquired with an Olympus stereomicroscope (Olympus Soft Imaging Solutions GmbH, The Netherlands). Accuracy of the hydrogel 3D constructs was also analyzed with SEM (Phenom Pro, Phenom-World, The Netherlands) at an acceleration voltage of 5−10 kV. Prior SEM imaging samples were gold-plated (2 nm) using a Q150R rotary-pumped sputter (Quorum Technologies, UK). Print fidelity was quantified using a relative value,
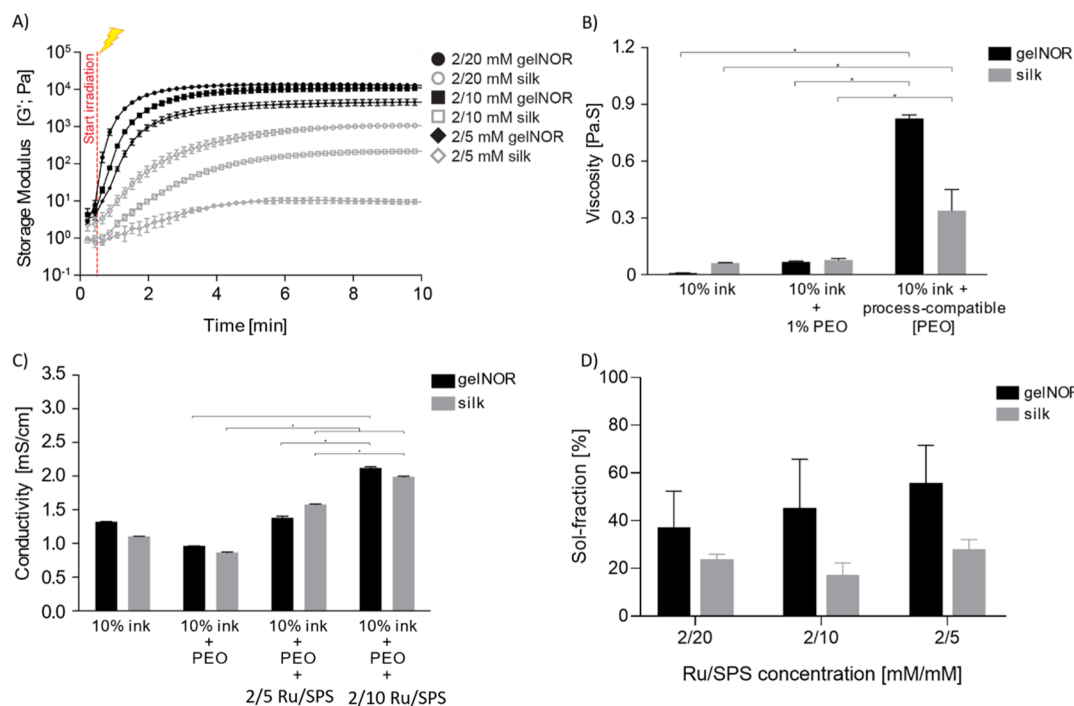
Figure 2. Physical–chemical properties of gelnor and silk fibroin bioink systems. (A) *In situ* photorheometry showing the storage modulus (G') of the bioinks as a function of time. Hydrogel samples were irradiated with visible light 30 s after the experiment started. (B) Viscosity changes as a function of the bioinks' PEO concentration. (C) Electrical conductivity of hydrogels as a function of both PEO and photoinitiator concentration. (D) Sol fraction as a function of Ru/SPS photoinitiator concentration.* indicates significant difference.

A_{ccpore}, expressed by the following index: $A_{\text{cc pore}} = A_{\text{fab}}/A_{\text{des}}$, where A_{fab} is the fabricated pore area and A_{des} is the designed pore area. The pore areas were quantified using Image J.

Cell Isolation and Culture. Equine tissue samples and cells were obtained from deceased horse donors, donated to science by their owners, according to the guidelines of the Institutional Animal Ethical Committee. Equine-derived bone marrow-derived mesenchymal stromal cells (MSCs) were isolated as previously described.[37] After isolation, the cells were cultured in MSC expansion medium consisting of DMEM + GlutaMAX (Gibco, 31966, The Netherlands), supplemented with fetal bovine serum (FBS, 10% v/v, Gibco, 10270, The Netherlands), penicillin/streptomycin (1%, Gibco, The Netherlands), L-ascorbic acid-2-phosphate (0.2×10^{-3} M, Sigma-Aldrich, The Netherlands), and basic fibroblast growth factor (1 ng/mL, PeproTech, United Kingdom); the medium was refreshed twice per week. The cells were expanded until passage 4 and used at a density of 10^8 cells/mL for both CEW and extrusion-based bioprinting.

Cell Viability. Cell viability in printed fibers was quantified through a LIVE/DEAD assay (Calcein AM, ethidium homodimer-1, Life Technologies, The Netherlands) using a confocal microscope (Leica SPX8, Leica Systems, The Netherlands) for imaging after 1, 3, and 7 days in culture ($n = 5$). Cast cell-laden hydrogels used as control groups were prepared using Teflon molds ($\varnothing = 6$ mm × $h = 2$ mm).

Immunofluorescent Stainings. At days 1 and 7 after CEW and extrusion bioprinting, the cell-laden constructs were fixed using 4% neutral buffered formalin. Following Triton-X membrane permeabilization, the samples were stained with phalloidin and DAPI. Images were captured using a Leica SP8X confocal microscope, and cell shapes were quantified using ImageJ.

Statistics. All results are presented as mean ± standard error. Statistical analyses were performed using GraphPad Prism 7.0 (GraphPad Software, USA). Differences between groups were assessed by a one-way ANOVA with a post hoc Bonferroni test. The differences were found to be significant when $p < 0.05$. For the FTIR analysis, the ratio between the areas under the asymmetric C−O−C and amide I peaks for each sample was compared to PEO-free

hydrogel controls, performing a one-way ANOVA with Bonferroni post hoc correction. Values of $p < 0.05$ indicated statistical significance.

■ RESULTS AND DISCUSSION

As a first step, the gelation kinetics, viscosity, and electrical conductivity of the CEW-compatible bioinks were tuned (Figure 1A). Clearly, fast gelation kinetics is paramount to form stable fibers with a reproducible diameter that can be effectively stacked into ordered 3D structures. Although this feature is also important for bioinks in conventional extrusion-based bioprinting, it poses a significant challenge for CEW, as the bioinks typically flow about 10−100 times faster within the electrohydrodynamic jet than within conventional extrusion-based bioprinting.[38] This results in a short latency time available to cross-link the jet before it is deposited onto the collector. Because of this short latency time, visible light-mediated thiol-ene click reactions and di-tyrosine oxidation photochemistries were used. More specifically, norbornene-modified gelatin (gelnor), which can form a hydrogel network through step growth polymerization in the presence of a multifunctional thiol cross-linker, and unmodified silk fibroin, which undergoes quick photochemical cross-linking because of the presence of tyrosine residues in its protein structure,[39] were selected as bioink platforms (Figure 1B). To accelerate the gelation kinetics, a two-component photoinitiator system was used, based on the mixture of tris(2,2-bipyridyl)-dichlororuthenium(II) hexahydrate and sodium persulfate (Ru/SPS). Such a two-component system has been recently introduced for both extrusion- and light-based bioprinting processes in the fabrication of large tissue constructs with complex geometry, through a photoreactive process, which is only marginally affected by oxygen inhibition.[16,36,40] Photo-rheological analysis at different Ru/SPS ratios confirmed
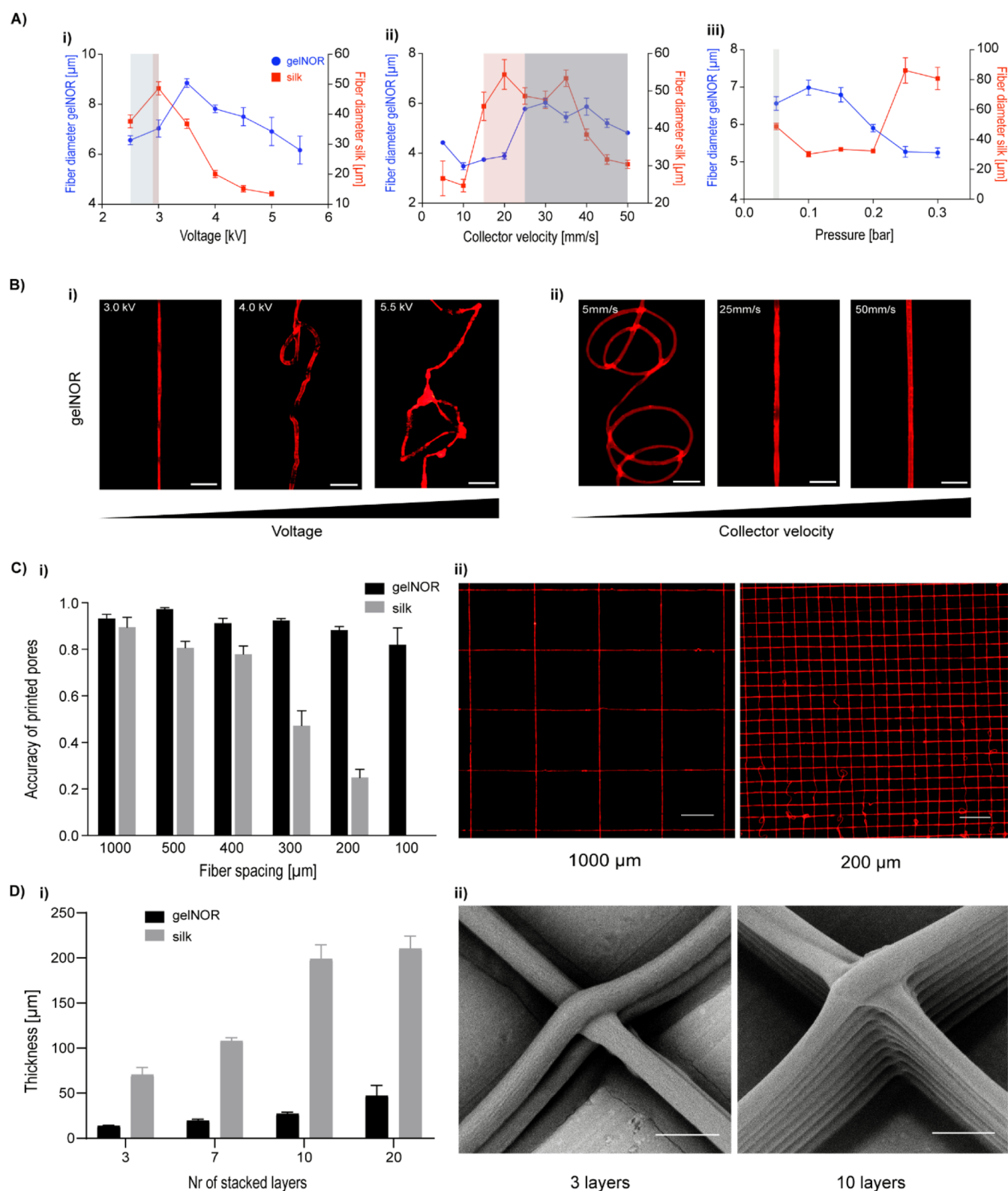
Figure 3. Influence of key CEW processing parameters on fiber collection and 3D patterning for both cell-free gelnor and silk fibroin hydrogel systems. (A) Effect of (i) voltage, (ii) collector velocity, and (iii) air pressure on fiber diameter. Printability window is represented by background colors. (B) Representative microscopic images of the effect of increasing (i) voltage and (ii) collector velocity on fiber morphology for the gelnor hydrogel system. Scale bar: 50 μm. (C) Print fidelity of fiber hydrogel 3D scaffolds. (Ci) Accuracy of printed pores, $A_{cc\ pore}$, as a function of scaffold pore size. $A_{cc\ pore}$ was determined using a relative value obtained by the ratio between the design and fabricated pore area. In the case of no deviation between the printed and designed pore areas, $A_{cc\ pore} = 1$. (Cii) Representative images of printed scaffolds with pore sizes of 1000 and 200 μm for gelnor hydrogel. Scale bar: 500 μm. (D) Scaffold thickness as a function of the number of stacked hydrogel layers. (Di) Final scaffold thickness and (Dii) representative SEM images of scaffolds with 3 and 10 layers showing perfectly stacked hydrogel fibers at the vertices of squared pores. Scale bar: 10 μm.

gelation of the gelnor and silk fibroin bioinks within less than 30 s and 1.5 min of exposure to visible light, respectively (Figure 2A). This underscores the potential of these material combinations as inks for CEW, in view of the short latency times during which fiber cross-linking must occur. It is important to mention that a slight increase in the storage modulus of the gelnor gels (but not of the silk gels) was observed, prior to the photo-exposure trigger. We attributed this to the high reactivity of the gelnor system, as recently described by Soliman and colleagues,[41] and to the potential photo-exposure while placing the hydrogel materials on the rheometer.

In parallel to the fast gelation requirement, CEW bioinks should possess high viscosity and moderate electrical conductivity to prevent Rayleigh instabilities and ensure steady jets. To enhance viscosity, gelnor and silk fibroin were blended with polyethylene oxide (PEO) at increasing concentrations (1−6% w/v). The viscosity of the gelnor−PEO and silk−PEO blends increased significantly compared to the gelnor- and silk fibroin-only solutions when PEO concentrations exceeded 3.4% v/v. Maximum viscosities of 0.8 and 0.4 Pa·s were obtained for gelnor and silk fibroin hydrogel systems with 6% v/v and 3.4% v/v PEO, respectively (Figure 2B). These PEO concentrations were required to prevent droplet formation and to thus allow a steady jet formation.

The electrical conductivity of the gelnor and silk fibroin hydrogels, with and without PEO, was considerably higher (0.9−1.3 mS/cm, Figure 2C) than that of semiconductive fluids (<10−11 mS/cm,[42,43]) that are considered ideal for steady jet formation under electrical fields. Nevertheless, our results demonstrate that these high conductivity values did not prevent stable jet formation, yet it did limit the continuous fiber collection to approximately 30 min. Based on our observations, this fabrication time was sufficient to collect satisfactory material volume without significant drying of the fibers. Additionally, the inclusion of 2/5 and 2/10 mM Ru/SPS resulted in a further increase of the conductivity of both hydrogel systems (1.5−2.3 mS/cm). This is likely due to the presence of sodium and persulfate ions from SPS in the aqueous medium of the ink. The presence of this compound determined a specific window within which the formation of a fluid jet at the spinneret was still possible (Figure 2C). Indeed, when the levels of SPS exceeded 10 mM, formation of a continuous jet was no longer observed, likely due to the excess of SPS ionic compounds and the resulting increase in electrical conductivity of the hydrogel. High cross-linking efficiency within such short latency time is of importance to ensure high printing resolution and cell embedding within the electro-written filament. Therefore, the effect of SPS and PEO on the cross-linking efficiency of both CEW bioinks was investigated by quantifying the sol fraction upon the formation of the polymer network. Both bioink systems, 10% gelnor + 6% PEO and 10% silk fibroin + 3.4% PEO, were able to form stable hydrogel fibers at 5 mM SPS concentration, which corresponded to an amount of uncross-linked polymer of approximately 50% (Figure 2D). This sol fraction value is likely due, on one hand, to the presence of PEO macro-molecules, which are not directly cross-linked in the hydrogel network, and on the other hand to the low SPS concentration used in the bioink. Ru/SPS mediates cross-linking of alkenes mainly *via* the generation of sulfate radicals,[36,44] whose concentration is dependent on the SPS content of the prepolymer solution. Lower sol fraction values could be

achieved for 20 and 10 mM SPS; however, continuous fiber deposition could not be obtained, which limited further 3D scaffold fabrication.

In order to allow controlled patterning of the fibers with the embedded cells, we then focused on fine-tuning the key CEW instrument parameters: applied voltage, collector velocity, and dispensing pressure, with respect to the fiber alignment and fiber diameter (Figure 3). The applied voltage was first studied at a constant collector velocity (25 mm/s) and applied pressure (0.05 bar), as the combination of these parameters allowed the consistent deposition of homogeneous fibers, that is, without a jet break and minimal oscillation of fiber diameter within a jet. An increase in both fiber straightness and diameter was observed between 2.5 and 3.0 kV, with fibers from both gelnor and silk fibroin hydrogel systems reaching full straightness (no visual fiber coiling) at 3.0 kV (Figure 3A(i),B(ii)). In contrast, coiling and reduction of the fiber diameter occurred when voltages between 3.0 and 5.0 kV were applied. The observed fiber coiling was likely due to an imbalance between the extrusion rate of the material and the velocity of the collector plate. Jet buckling and consequent fiber coiling typically occur when the jet velocity is higher than the collection velocity, as previously described for other direct writing electrofabrication methods.[45,46] By increasing the collector velocity from 25 to 50 mm/s, a reduction in fiber coiling and fiber diameter was consequently observed (Figure 3A(ii),B(ii)). This suggests that an adequate balance between extrusion rate and collection velocity can prevent jet buckling and simultaneously reduce fiber diameter. For collector velocities between 25 and 50 mm/s, fiber diameters between 3 and 6 μm for gelnor, and 40−45 μm for silk fibroin (Figure 3A(ii)), were obtained. The higher fiber diameter for the silk hydrogel system is most likely attributed to the precursor solution showing a viscosity about twofold lower than that of the gelnor system. Regardless of these differences, the obtained fiber diameters are 1 to 2 orders of magnitude smaller than the fiber sizes previously reported for extrusion-based bioprinting (≈200 μm).[47,48] Interestingly, the obtained fiber diameters approximate the size of a single cell (animal cell size ∼ 10 μm) and were suitable for cell encapsulation. The effect of the dispensing pressure was also investigated, yet straight fiber alignment was only observed within a narrow pressure range (Figure 3A(iii)). Because of the low viscosity of both hydrogel systems, dispensing pressures above 0.05 bar resulted in excessive flow rates and consequent fiber coiling and fiber diameter oscillation. An overview of the effect of key hydrogel bioink material properties and CEW processing parameters on jet formation, as well as of the physical mechanisms governing the CEW process, is provided in Figures S1 and S6, respectively.

Next, the patterning capacity of both gelnor and silk hydrogels was investigated by manufacturing 3D scaffolds with square pore geometries of varying pore sizes, from 100 μm to 1000 μm, and varying scaffold thicknesses, from 1 to 30 layers (Figure 3C(i,ii)). All scaffolds were fabricated under optimized fabrication parameters, that is, constant collector velocity of [25, 30] mm/s, voltages of 2.5 (gelnor) and 3.0 (silk), air pressure of 0.05 bar, and cross-linking time with visible light (400−450 nm) during jet collection and after printing for approx. 5 min. Scaffolds with precisely configured square pores were obtained with minimum pore sizes of 100 μm for gelnor and 400 μm for silk (accuracy of printed pores > 0.8). Smaller pore sizes could also be achieved, but this compromised the
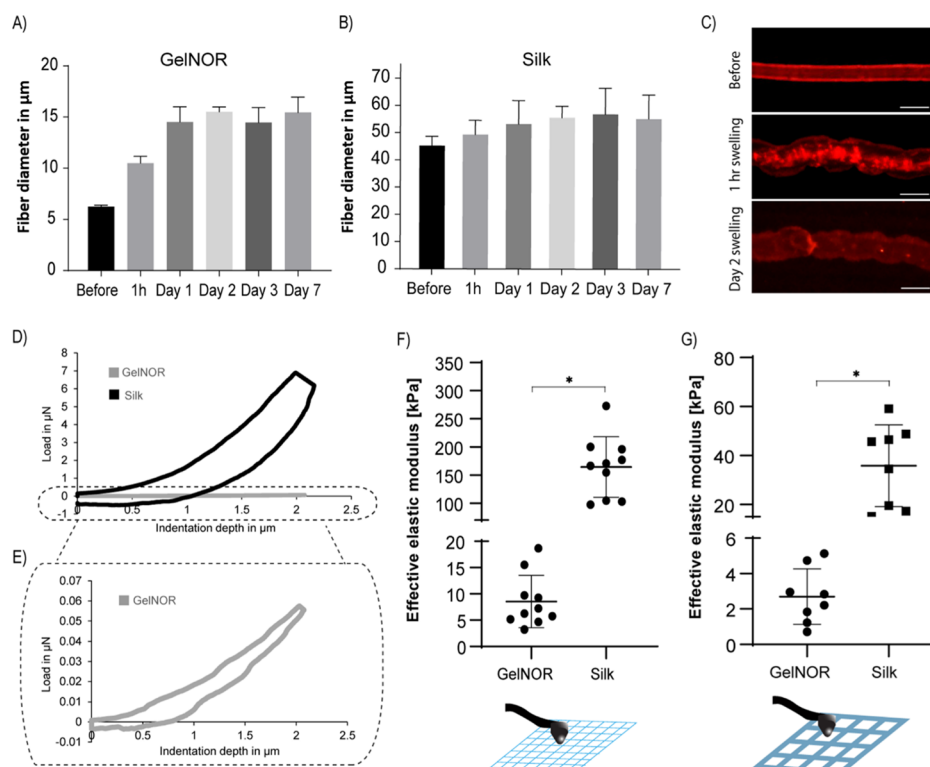
Figure 4. Swelling and mechanical characteristics of CEW hydrogels fibers. Swelling of (A) gelnor and (B) silk fibroin-based cell-free hydrogel fiber before and after 1 h, 1,, 2, 3, and 7 days incubation in PBS. (C) Representative images of swollen gelnor fibers before and after 1 h and 2 days of swelling. (D,E) Representative loading and unloading curves of CEW gelnor and silk-based cell-free scaffolds measured by nanoindentation. Curves have been averaged over at least three measurements. (F) Effective stiffness of CEW gelnor and silk fibroin-based cell-free scaffolds and (G) comparison with the scaffolds of same composition obtained by conventional extrusion bioprinting. All nanoindentation experiments were performed on scaffolds after 1 day of PBS immersion (equilibrium swelling).

accuracy of printed constructs, resulting in higher deviations between the printed constructs and their digitally designed counterparts (data not shown). The lower print fidelity, and consequently larger pore sizes obtained for the silk ink, is most likely attributed to the lower viscosity and slower reactivity of this system. These two aspects combined resulted in less stable material collection during printing.

In addition, the ability to form scaffolds with curved fibers instead of straight fibers was also demonstrated (Figure S2). Both bioink systems allowed the accurate writing of hemispherical shaped fiber scaffolds with a minimum interfiber distance of 200 μm. We further observed that scaffolds with thicknesses of 50 and 200 μm for the gelnor and silk hydrogel systems, respectively, could be fabricated without significantly affecting the printing accuracy (Figure 3D(i,ii)). Above these thicknesses, accurate fiber placement and stacking were hampered, likely due to the residual charges accumulated in and onto the electrified jets,[49,50] resulting in repulsive Coulomb interactions between the new and previously deposited fibers. Importantly, the hydrogel systems and the CEW process allowed the fabrication of regularly structured biocompatible hydrogel scaffolds with unprecedented high resolution and geometrical accuracies. To the best of our knowledge, no other nozzle-based biofabrication approach or MEW technology has been able to process natural-derived protein-based hydrogels with a similar control over the spatial resolution of the fibers (Table S1).

Subsequently, the swelling and mechanical characteristics of gelnor and silk fibroin CEW scaffolds were investigated (Figure 4). The swelling behavior was studied by measuring the

diametral changes of single CEW fibers when subjected to an aqueous environment over 7 days (Figure 4A−C). The diameter of gelnor fibers increased by approximately 2.5-fold compared to that on day 0, reaching a maximum diameter of 15.3 ± 0.5 μm (Figure 4A,C), whereas silk fibroin fibers displayed an increase of only 1.1-fold, reaching a maximum diameter of 55.9 ± 9.5 μm (Figure 4B). Interestingly, both gelnor and silk fibroin fibers reached the equilibrium swelling at day 1, after which no change in morphology was observed until day 7. After day 7, small fiber breakage and loss of fiber morphological structure started to be observed in both material systems, which indicate partial material degradation. This limited stability in aqueous environments after 7 days could be improved by increasing the cross-link density (i.e., polymer concentration and irradiation time), although at the cost of potentially reducing viability of encapsulated cells and their ability to synthetize new ECM. Further, the mechanical properties of gelnor and silk fibroin CEW scaffolds were determined by nanoindentation testing carried out on CEW scaffolds at equilibrium swelling (Figure 4D−G). This mechanical testing method was selected because of its sensitivity to measure forces in the range of nano- to micro-Newtons and the suitability to characterize small-sized constructs, that is, on the scale of nano- to micrometers. The load−displacement curves of gelnor and silk fibroin CEW scaffolds with three layers were compared with those of the scaffolds of the same composition prepared by conventional extrusion-based printing (Figure 4D, only representative images of CEW scaffolds are shown). We observed that the effective elastic modulus of gelnor scaffolds (CEW, 8.5 ± 4.9
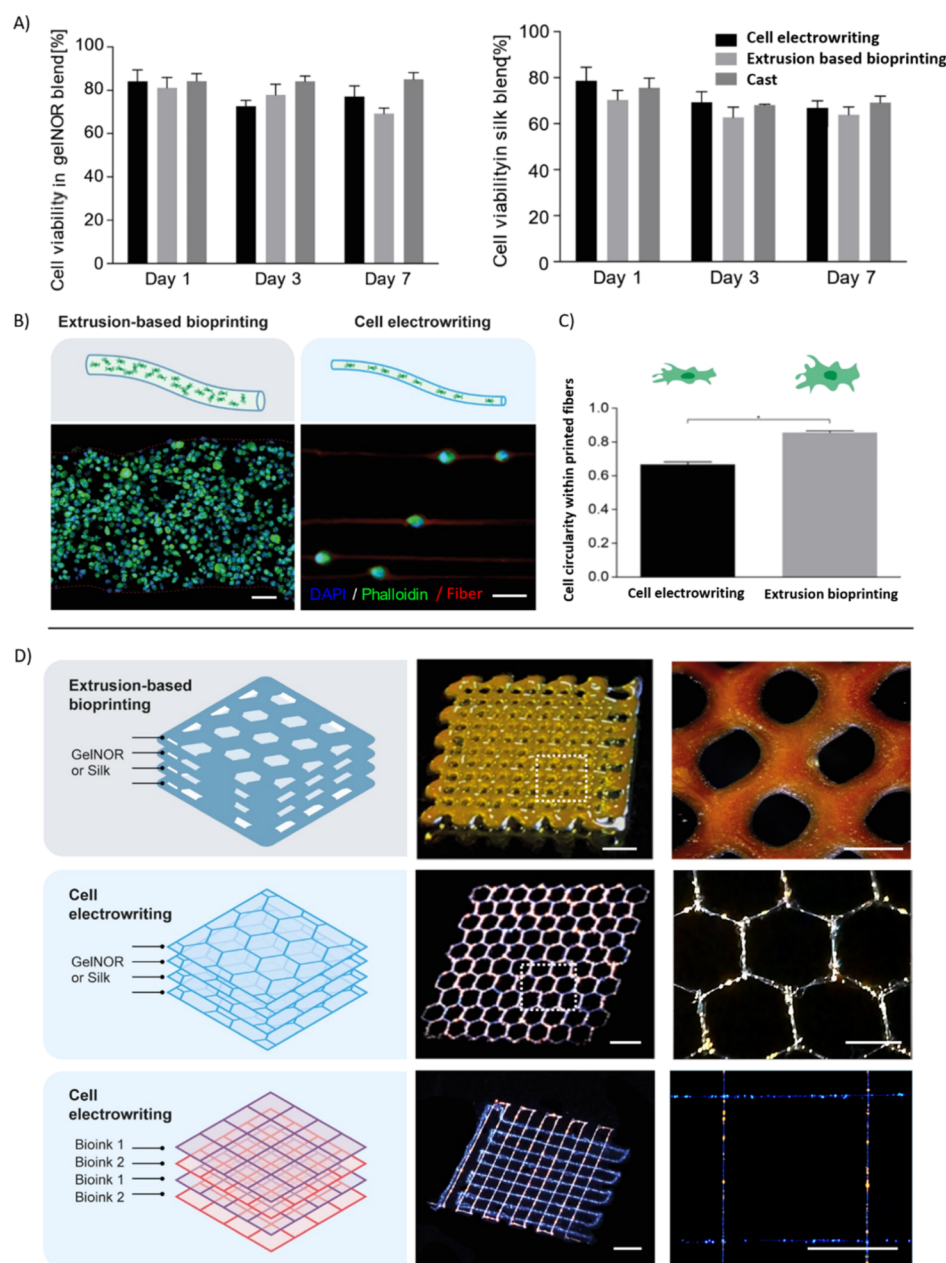
Figure 5. CEW of complex-shaped cell-laden fiber scaffolds. (A) Cell viability of gelnor and silk fibroin-based cell-laden scaffolds after 1, 3, and 7 days of *in vitro* culture. Cell electrowritten scaffolds exhibited high cell viability (>70%) for both hydrogel systems, similar to the conventional extrusion-based bioprinting and manual hydrogel casting. (B,C) Cell distribution and morphology were examined on gelnor-based cell-laden scaffolds and compared with conventional extrusion bioprinting. Cell electrowritten fibers exhibited single cells accurately aligned along the fiber pattern. Meanwhile, extrusion-bioprinted fibers exhibited multiple cells distributed homogeneously along the thickness of the filament. Scale bar: 20 μm. (D) Complex shape patterning of representative gelnor-based electrowritten scaffolds with fluorescent nanoparticles. Cell electrowritten hexagon-shaped 3D scaffolds exhibited 2 times higher printing accuracy than the extruded printed scaffolds. CEW also allowed simultaneous printing of multiple bioinks in one single construct. Scale bars: 800 μm (left panels) and 400 μm (right panels).

kPa; extrusion, 2.7 ± 1.5 kPa) was significantly lower than that of silk scaffolds (CEW, 164.3 ± 53.8 kPa; extrusion, 35.8 ± 16.7 kPa) (Figure 4F,G). Notably, the effective stiffness of CEW scaffolds was 3 (gelnor) to 4.5 (silk) times higher than that found for extruded printed scaffolds. Such differences are likely due to the higher shear-induced alignment by the CEW process than by the conventional extrusion printing, which led to the generation of polymer fibers with a high degree of orientation and reduced number of polymer entanglements. In addition, the obtained effective stiffness is comparable to that reported for other alginate- and gelatin-based materials (4

kPa−20 MPa)[51,52] but significantly lower for silk-based hydrogels (24−1864 MPa)[53] processed by other electrohydrodynamic processes (see also Table S1). This is likely due to the methanol treatment used to stabilize silk fibroin fibers obtained with other electrohydrodynamic techniques, which induces the rearrangement of silk fibroin chains into β-sheet crystals. Although this treatment conveys the silk mechanical properties similar to those of native silk fibers, it would not be suitable for the stabilization of cell-laden fibers.[54] Importantly, all silk scaffolds showed a greater overall energy absorption than the gelnor scaffolds, as observed from the different load−

displacement response curves (Figure 4D−E). This confirms the improved ductile behavior of the presented silk fibroin bioink system in comparison with the conventionally used alginate hydrogel systems for electrohydrodynamic processes.

Subsequently, the ability to pattern gelatin and silk fibroin hydrogels into 3D organized microfiber networks with encapsulated cells was assessed. For this, bone marrow-derived MSCs were mixed within the ink precursors. Cell concentrations up to 108 cells/mL could successfully be processed, and cell-laden electrowritten microfibers could be obtained. Viability of the electrowritten cells was determined at 1, 3, and 7 days of culture post printing, revealing a high ratio of living cells (>70% at all time points) for both gelnor and silk fibroin bioinks (Figure 5A). These values were comparable to those observed for conventional extrusion-based bioprinted and cast controls and were in line with previous works on different electrohydrodynamic techniques (Table S1). Furthermore, the presence of the viscosity enhancer PEO in the gelnor and silk fibroin-based CEW bioinks before and after incubation in PBS for 0, 24, and 72 h was studied (Figure S3). Analysis performed on the FTIR spectra of gelnor revealed the presence of peaks characteristic of PEG−thiol, namely the peaks indicative of the asymmetric and symmetric C−O−C stretching ($\approx$1090 and 845 cm^{-1}, respectively), representative of the incorporation of the PEG−thiol cross-linker within the polymer network (Figure S3A). Although the inherent presence of such molecules within the gelatin hydrogels renders the PEO removal upon washing of the gels difficult to assess by means of FTIR, the analysis of the peak area between the ether peaks and amide I ($\approx$1650 cm^{-1}) suggests that PEO residues may persist within the hydrogel after 3 days of washing (Figure S3C). This is possibly due to the entrapment of PEO chains within the gelatin network. Although these data suggest that different washing protocols may be required to completely remove PEO, no significant effect on the cell metabolic activity was detected after 3 days of culture, indicating the overall safety of having this supplemental molecule as the viscosity enhancer (Figure 5A). Conversely, in the case of the silk fibroin hydrogels, PEO removal after 1 day of incubation in PBS was demonstrated, with the ratio between the area under the ether C−O−C stretching peak and the amide I band reaching values comparable to those of pristine silk (Figure S3B−D). Taken together, these data show that the CEW process preserves cell viability, suggesting that the relatively high viscosity of the bioinks, the applied electric field, and the resulting shear stresses within the electrohydrodynamic jet did not induce significant damage to the cells. This is in agreement with previous works, which also indicated that living cells could be safely electrospun, reaching a minimum size of approximately 10 μm in diameter, even though in such setups, differently from CEW, limited patterning control was observed (Table S1).[18,24,55]

We further investigated cell distribution and morphology within the gelnor hydrogel system, as we hypothesized that smaller fiber diameters could alter these parameters substantially. In contrast to what is observed for the distribution of cells within large ($\approx$300 μm) hydrogel filaments obtained through conventional extrusion-based bioprinting, printed cells in gelnor through the CEW process are accurately aligned following the deposition pattern of the fibers (Figure 5B). An interesting feature of the gelnor CEW process is that each printed microfiber (diameter $\approx$ 2−10 μm) is significantly smaller than the size of an individual MSC in suspension

($\approx$10−30 μm).[56] Small, submicron features, such as grooves, pillars, and microfibers, are generally known to greatly affect cell morphology *via* contact guidance and spatial constriction.[57] However, from a morphological point of view, the electrowritten cells showed only a slight cytoskeletal deformation, yet no significant morphological changes in the nucleus, compared to the cells embedded in extrusion-based printed fibers, as observed by measuring cell circularity as a shape descriptor (Figure 5C). Interestingly, the bioinks, rather than providing a strict confinement for the embedded cells, simply appear to accommodate for the cell size, encapsulating them in a bead-and-necklace-like conformation.

In addition, fluorescent microparticles, with the size comparable to that of MSCs, were used to facilitate the visualization of "cell-laden" constructs with more complex geometries and material combinations (Figure 5D). The unique patterning capabilities of the CEW process were demonstrated by printing complex hexagonal pore structures (accuracy of printed pores > 0.8), which could not be reproduced by conventional extrusion-based bioprinting (accuracy of printed pores < 0.4) (Figures 5D, S5). The potential of the CEW process for multimaterial fiber scaffold fabrication was further investigated by simultaneous printing of two gelnor bioinks loaded with fluorescent particles displaying different emission wavelengths. Well-organized microstructures with square-shaped pores were successfully obtained (Figure 5D). This versatility of the CEW process is a powerful characteristic that can aid the generation of more relevant ECM-like microenvironments that combine different materials and cell types. Another important implication of our results is the potential development of multiple tissue-type microenvironments, as the investigated cells, MSCs, possess the ability to differentiate toward different lineages (*e.g.*, myoblasts, tendons, and neural-like cells). However, the remaining challenge is to maintain both the shape and stability of the fabricated cell-laden fibers over culturing periods longer than 7 days. Because of the reduced fiber size (combined with potentially the relatively high sol fraction in the gelnor bioinks) and enzymatic activity during culture, strategies to accurately control the degradation kinetics and mechanical stability may be required.

CONCLUSIONS

In summary, the unique biocompatibility of both the gelnor and silk fibroin materials, their promising mechanical performance when compared with conventional extrusion bioprinting, the reduced cell-laden fiber sizes (5−40 μm), and the unprecedented resolution and patterning precision open promising avenues for the high-resolution printing of labile biological moieties and living cells. These remarkable features of the novel photoresponsive hydrogel bioinks and CEW process will allow to create microstructure scaffolds that can better resemble cellular microenvironments for RM (*e.g.*, muscle fibers, tendons, and nerve networks) and organ-on-a chip models. One of the fascinating applications of CEW is the creation of unique cell culture platforms for applications in developmental biology and drug discovery because the cellular microenvironment could now be further controlled by the resulting cell-laden fiber size, material composition, scaffold architecture, and mechanical properties.

■ ASSOCIATED CONTENT

Ⓢ Supporting Information

The Supporting Information is available free of charge at https://pubs.acs.org/doi/10.1021/acs.biomac.0c01577.

CEW fabrication window, representative microscopy images of curved CEW fibers, FTIR data, representative fluorescence images of cells on gelnor-based cell-laden scaffolds, additional printing accuracy of gelnor scaffolds, schematic representation of the custom-made CEW setup and working principle, and comparison of the existent electrohydrodynamic techniques using polymer and hydrogel solutions (PDF)

■ AUTHOR INFORMATION

Corresponding Author

Miguel Castilho − Department of Orthopedics, University Medical Center Utrecht, Utrecht University, 3508 GA Utrecht, The Netherlands; Department of Biomedical Engineering, Eindhoven University of Technology, 5612 AZ Eindhoven, The Netherlands; ⓘ orcid.org/0000-0002-4269-5889; Email: M.DiasCastilho@umcutrecht.nl

Authors

Riccardo Levato − Department of Orthopedics, University Medical Center Utrecht and Department of Clinical Sciences, Faculty of Veterinary Medicine, Utrecht University, 3508 GA Utrecht, The Netherlands; ⓘ orcid.org/0000-0002-3795-3804

Paulina Nunez Bernal − Department of Orthopedics, University Medical Center Utrecht, Utrecht University, 3508 GA Utrecht, The Netherlands

Mylène de Ruijter − Department of Orthopedics, University Medical Center Utrecht, Utrecht University, 3508 GA Utrecht, The Netherlands

Christina Y. Sheng − Department of Orthopedics, University Medical Center Utrecht, Utrecht University, 3508 GA Utrecht, The Netherlands

Joost van Duijn − Department of Orthopedics, University Medical Center Utrecht, Utrecht University, 3508 GA Utrecht, The Netherlands

Susanna Piluso − Department of Orthopedics, University Medical Center Utrecht, Utrecht University, 3508 GA Utrecht, The Netherlands; Department of Developmental BioEngineering, Technical Medical Centre, University of Twente, 7522 NB Enschede, The Netherlands; ⓘ orcid.org/0000-0003-0508-711X

Keita Ito − Department of Orthopedics, University Medical Center Utrecht, Utrecht University, 3508 GA Utrecht, The Netherlands; Department of Biomedical Engineering, Eindhoven University of Technology, 5612 AZ Eindhoven, The Netherlands

Jos Malda − Department of Orthopedics, University Medical Center Utrecht and Department of Clinical Sciences, Faculty of Veterinary Medicine, Utrecht University, 3508 GA Utrecht, The Netherlands; ⓘ orcid.org/0000-0002-9241-7676

Complete contact information is available at:
https://pubs.acs.org/10.1021/acs.biomac.0c01577

Author Contributions

[1]M.C. and R.L. contributed equally to this work. The manuscript was written through contributions of all authors.

All authors have given approval to the final version of the manuscript.

Notes

The authors declare no competing financial interest.

■ ACKNOWLEDGMENTS

■ REFERENCES

(1) Groll, J.; Boland, T.; Blunk, T.; Burdick, J. A.; Cho, D.-W.; Dalton, P. D.; Derby, B.; Forgacs, G.; Li, Q.; Mironov, V. A.; Moroni, L.; Nakamura, M.; Shu, W.; Takeuchi, S.; Vozzi, G.; Woodfield, T. B. F.; Xu, T.; Yoo, J. J.; Malda, J. Biofabrication: Reappraising the Definition of an Evolving Field. *Biofabrication* **2016**, *8*, 013001.

(2) Brassard, J. A.; Lutolf, M. P. Engineering Stem Cell Self-Organization to Build Better Organoids. *Cell Stem Cell* **2019**, *24*, 860−876.

(3) Moroni, L.; Burdick, J. A.; Highley, C.; Lee, S. J.; Morimoto, Y.; Takeuchi, S.; Yoo, J. J. Biofabrication Strategies for 3D in Vitro Models and Regenerative Medicine. *Nat. Rev. Mater.* **2018**, *3*, 21−37.

(4) Levato, R.; Jungst, T.; Scheuring, R. G.; Blunk, T.; Groll, J.; Malda, J. Shape to Function. *Adv. Mater.* **2020**, *32*, 1906423.

(5) No, Y. J.; Castilho, M.; Ramaswamy, Y.; Zreiqat, H. Role of Biomaterials and Controlled Architecture on Tendon/Ligament Repair and Regeneration. *Adv. Mater.* **2019**, *32*, 1904511.

(6) Castilho, M.; de Ruijter, M.; Beirne, S.; Villette, C.; Ito, K.; Wallace, G.; Malda, J. Multitechnology Biofabrication: A New Approach for the Manufacturing of Functional Tissue Structures? *Trends Biotechnol.* **2020**, *38*, 1316−1328.

(7) Sart, S.; Ma, T.; Li, Y. Preconditioning Stem Cells for In Vivo Delivery. *BioRes. Open Access* **2014**, *3*, 137−149.

(8) Vining, K. H.; Mooney, D. J. Mechanical Forces Direct Stem Cell Behaviour in Development and Regeneration. *Nat. Rev. Mol. Cell Biol.* **2017**, *18*, 728−742.

(9) Charras, G.; Sahai, E. Physical Influences of the Extracellular Environment on Cell Migration. *Nat. Rev. Mol. Cell Biol.* **2014**, *15*, 813−824.

(10) Castilho, M.; van Mil, A.; Maher, M.; Metz, C. H. G.; Hochleitner, G.; Groll, J.; Doevendans, P. A.; Ito, K.; Sluijter, J. P. G.; Malda, J. Melt Electrowriting Allows Tailored Microstructural and Mechanical Design of Scaffolds to Advance Functional Human Myocardial Tissue Formation. *Adv. Funct. Mater.* **2018**, *28*, 1803151.

(11) Deglincerti, A.; Etoc, F.; Guerra, M. C.; Martyn, I.; Metzger, J.; Ruzo, A.; Simunovic, M.; Yoney, A.; Brivanlou, A. H.; Siggia, E.;

Warmflash, A. Self-Organization of Human Embryonic Stem Cells on Micropatterns. *Nat. Protoc.* **2016**, *11*, 2223−2232.

(12) Luo, T.; Mohan, K.; Iglesias, P. A.; Robinson, D. N. Molecular Mechanisms of Cellular Mechanosensing. *Nat. Mater.* **2013**, *12*, 1064−1071.

(13) Norotte, C.; Marga, F. S.; Niklason, L. E.; Forgacs, G. Scaffold-Free Vascular Tissue Engineering Using Bioprinting. *Biomaterials* **2009**, *30*, 5910−5917.

(14) Liu, W.; Zhang, Y. S.; Heinrich, M. A.; De Ferrari, F.; Jang, H. L.; Bakht, S. M.; Alvarez, M. M.; Yang, J.; Li, Y.-C.; Trujillo-de Santiago, G.; Miri, A. K.; Zhu, K.; Khoshakhlagh, P.; Prakash, G.; Cheng, H.; Guan, X.; Zhong, Z.; Ju, J.; Zhu, G. H.; Jin, X.; Shin, S. R.; Dokmeci, M. R.; Khademhosseini, A. Rapid Continuous Multi-material Extrusion Bioprinting. *Adv. Mater.* **2017**, *29*, 1604630.

(15) Yanez, M.; Rincon, J.; Dones, A.; De Maria, C.; Gonzales, R.; Boland, T. Vivo Assessment of Printed Microvasculature in a Bilayer Skin Graft to Treat Full-Thickness Wounds. *Tissue Eng., Part A* **2015**, *21*, 224.

(16) Lim, K. S.; Levato, R.; Costa, P. F.; Castilho, M. D.; Alcala-Orozco, C. R.; Van Dorenmalen, K. M. A.; Melchels, F. P. W.; Gawlitta, D.; Hooper, G. J.; Malda, J.; Woodfield, T. B. F. Bio-Resin for High Resolution Lithography-Based Biofabrication of Complex Cell-Laden Constructs. *Biofabrication* **2018**, *10*, 034101.

(17) Dobos, A.; Van Hoorick, J.; Steiger, W.; Gruber, P.; Markovic, M.; Andriotis, O. G.; Rohatschek, A.; Dubruel, P.; Thurner, P. J.; Van Vlierberghe, S.; Baudis, S.; Ovsianikov, A. Thiol−Gelatin−Norbornene Bioink for Laser-Based High-Definition Bioprinting. *Adv. Healthcare Mater.* **2019**, *9*, 1900752.

(18) Ehler, E.; Jayasinghe, S. N. Cell Electrospinning Cardiac Patches for Tissue Engineering the Heart. *Analyst* **2014**, *139*, 4449.

(19) Hu, M.; Deng, R.; Schumacher, K. M.; Kurisawa, M.; Ye, H.; Purnamawati, K.; Ying, J. Y. Hydrodynamic Spinning of Hydrogel Fibers. *Biomaterials* **2010**, *31*, 863−869.

(20) Chen, H.; Liu, Y.; Hu, Q. A Novel Bioactive Membrane by Cell Electrospinning. *Exp. Cell Res.* **2015**, *338*, 261−266.

(21) He, J.; Zhao, X.; Chang, J.; Li, D. Microscale Electro-Hydrodynamic Cell Printing with High Viability. *Small* **2017**, *13*, 1702626.

(22) Zhao, X.; He, J.; Xu, F.; Liu, Y.; Li, D. Electrohydrodynamic Printing a Potential Tool for High-Resolution Hydrogel/Cell Patterning. *Virtual Phys. Prototyp.* **2016**, *11*, 57−63.

(23) Li, J.; Wu, S.; Kim, E.; Yan, K.; Liu, H.; Liu, C.; Dong, H.; Qu, X.; Shi, X.; Shen, J.; Bentley, W. E.; Payne, G. F. Electrobiofabrication: Electrically Based Fabrication with Biologically Derived Materials. *Biofabrication* **2019**, *11*, 032002.

(24) Sampson, S. L.; Saraiva, L.; Gustafsson, K.; Jayasinghe, S. N.; Robertson, B. D. Cell Electrospinning: An in Vitro and in Vivo Study. *Small* **2014**, *10*, 78.

(25) Jayasinghe, S. N.; Auguste, J.; Scotton, C. J. Platform Technologies for Directly Reconstructing 3D Living Biomaterials. *Adv. Mater.* **2015**, *27*, 7794.

(26) Yeo, M.; Ha, J.; Lee, H.; Kim, G. Fabrication of HASCs-Laden Structures Using Extrusion-Based Cell Printing Supplemented with an Electric Field. *Acta Biomater.* **2016**, *38*, 33−43.

(27) Li, X.; Li, Z.; Wang, L.; Ma, G.; Meng, F.; Pritchard, R. H.; Gill, E. L.; Liu, Y.; Huang, Y. Y. S. Low-Voltage Continuous Electro-spinning Patterning. *ACS Appl. Mater. Interfaces* **2016**, *8*, 32120−32131.

(28) Liaudanskaya, V.; Gasperini, L.; Maniglio, D.; Motta, A.; Migliaresi, C. Assessing the Impact of Electrohydrodynamic Jetting on Encapsulated Cell Viability, Proliferation, and Ability to Self-Assemble in Three-Dimensional Structures. *Tissue Eng., Part C* **2015**, *21*, 631.

(29) Nahm, D.; Weigl, F.; Schaefer, N.; Sancho, A.; Frank, A.; Groll, J.; Villmann, C.; Schmidt, H.-W.; Dalton, P. D.; Luxenhofer, R. A Versatile Biomaterial Ink Platform for the Melt Electrowriting of Chemically-Crosslinked Hydrogels. *Mater. Horiz.* **2020**, *7*, 928.

(30) Jordahl, J. H.; Solorio, L.; Sun, H.; Ramcharan, S.; Teeple, C. B.; Haley, H. R.; Lee, K. J.; Eyster, T. W.; Luker, G. D.; Krebsbach, P.

H.; Lahann, J. 3D Jet Writing: Functional Microtissues Based on Tessellated Scaffold Architectures. *Adv. Mater.* **2018**, *30*, 1707196.

(31) Wu, D. J.; Vonk, N. H.; Lamers, B. A. G.; Castilho, M.; Malda, J.; Hoefnagels, J. P. M.; Dankers, P. Y. W. Anisotropic Hygro-Expansion in Hydrogel Fibers Owing to Uniting 3D Electrowriting and Supramolecular Polymer Assembly. *Eur. Polym. J.* **2020**, *141*, 110099.

(32) Mackiewicz, Z.; Konttinen, Y. T.; Kaivosoja, E.; Stegajev, V.; Wagner, H. D.; Lévón, J.; Tiainen, V. M. Extracellular Matrix and Tissue Regeneration. In *Regenerative Medicine-from Protocol to Patient: 1. Biology of Tissue Regeneration*, 3rd ed, 2016.

(33) Gu, L.; Jiang, Y.; Hu, J. Scalable Spider-Silk-Like Supertough Fibers Using a Pseudoprotein Polymer. *Adv. Mater.* **2019**, *31*, 1904311.

(34) Rockwood, D. N.; Preda, R. C.; Yücel, T.; Wang, X.; Lovett, M. L.; Kaplan, D. L. Materials Fabrication from Bombyx Mori Silk Fibroin. *Nat. Protoc.* **2011**, *6*, 1612−1631.

(35) Mũnoz, Z.; Shih, H.; Lin, C. C. Gelatin Hydrogels Formed by Orthogonal Thiol-Norbornene Photochemistry for Cell Encapsula-tion. *Biomater. Sci.* **2014**, *2*, 1063−1072.

(36) Lim, K. S.; Schon, B. S.; Mekhileri, N. V.; Brown, G. C. J.; Chia, C. M.; Prabakar, S.; Hooper, G. J.; Woodfield, T. B. F. New Visible-Light Photoinitiating System for Improved Print Fidelity in Gelatin-Based Bioinks. *ACS Biomater. Sci. Eng.* **2016**, *2*, 1752−1762.

(37) Mouser, V. H. M.; Abbadessa, A.; Levato, R.; Hennink, W. E.; Vermonden, T.; Gawlitta, D.; Malda, J. Development of a Thermosensitive HAMA-Containing Bio-Ink for the Fabrication of Composite Cartilage Repair Constructs. *Biofabrication* **2017**, *9*, 015026.

(38) Montinaro, M.; Fasano, V.; Moffa, M.; Camposeo, A.; Persano, L.; Lauricella, M.; Succi, S.; Pisignano, D. Sub-Ms Dynamics of the Instability Onset of Electrospinning. *Soft Matter* **2015**, *11*, 3424−3431.

(39) Cui, X.; Soliman, B. G.; Alcala-Orozco, C. R.; Li, J.; Vis, M. A. M.; Wise, S. G.; Levato, R.; Woodfield, T. B. F.; Rnjak-Kovacina, J.; Lim, K. S.; Rnjak-Kovacina, J.; Lim, K. Rapid Photocrosslinking of Silk Hydrogels with High Cell Density and Enhanced Shape Fidelity. *Adv. Healthcare Mater.* **2020**, *9*, 1901667.

(40) Bertlein, S.; Brown, G.; Lim, K. S.; Jungst, T.; Boeck, T.; Blunk, T.; Tessmar, J.; Hooper, G. J.; Woodfield, T. B. F.; Groll, J. Thiol−Ene Clickable Gelatin: A Platform Bioink for Multiple 3D Biofabrication Technologies. *Adv. Mater.* **2017**, *29*, 1703404.

(41) Soliman, B. G.; Lindberg, G. C. J.; Jungst, T.; Hooper, G. J.; Groll, J.; Woodfield, T. B. F.; Lim, K. S. Stepwise Control of Crosslinking in a One-Pot System for Bioprinting of Low-Density Bioinks. *Adv. Healthcare Mater.* **2020**, *9*, 1901544.

(42) Gambhire, P.; Thaokar, R. M. Role of Conductivity in the Electrohydrodynamic Patterning of Air-Liquid Interfaces. *Phys. Rev. E: Stat., Nonlinear, Soft Matter Phys.* **2012**, *86*, 036301.

(43) Hayati, I.; Bailey, A. I.; Tadros, T. F. Mechanism of Stable Jet Formation in Electrohydrodynamic Atomization. *Nature* **1986**, *319*, 41−43.

(44) Lim, K. S.; Abinzano, F.; Bernal, P. N.; Albillos Sanchez, A.; Atienza-Roca, P.; Otto, I. A.; Peiffer, Q. C.; Matsusaki, M.; Woodfield, T. B. F.; Malda, J.; Levato, R. One-Step Photoactivation of a Dual-Functionalized Bioink as Cell Carrier and Cartilage-Binding Glue for Chondral Regeneration. *Adv. Healthcare Mater.* **2020**, *9*, 1901792.

(45) Hochleitner, G.; Youssef, A.; Hrynevich, A.; Haigh, J. N.; Jungst, T.; Groll, J.; Dalton, P. D. Fibre Pulsing during Melt Electrospinning Writing. *BioNanoMaterials* **2016**, *17*, 159.

(46) Castilho, M.; Feyen, D.; Flandes-Iparraguirre, M.; Hochleitner, G.; Groll, J.; Doevendans, P. A. F.; Vermonden, T.; Ito, K.; Sluijter, J. P. G.; Malda, J. Melt Electrospinning Writing of Poly-Hydroxyme-thylglycolide-Co-ε-Caprolactone-Based Scaffolds for Cardiac Tissue Engineering. *Adv. Healthcare Mater.* **2017**, *6*, 1700311.

(47) Liu, W.; Heinrich, M. A.; Zhou, Y.; Akpek, A.; Hu, N.; Liu, X.; Guan, X.; Zhong, Z.; Jin, X.; Khademhosseini, A.; Zhang, Y. S. Extrusion Bioprinting of Shear-Thinning Gelatin Methacryloyl Bioinks. *Adv. Healthcare Mater.* **2017**, *6*, 1601451.

(48) de Ruijter, M.; Ribeiro, A.; Dokter, I.; Castilho, M.; Malda, J. Simultaneous Micropatterning of Fibrous Meshes and Bioinks for the Fabrication of Living Tissue Constructs. *Adv. Healthcare Mater.* **2019**, *8*, 1800418.

(49) Collins, G.; Federici, J.; Imura, Y.; Catalani, L. H. Charge Generation, Charge Transport, and Residual Charge in the Electrospinning of Polymers: A Review of Issues and Complications. *J. Appl. Phys.* **2012**, *111*, 044701.

(50) Wunner, F. M.; Wille, M.-L.; Noonan, T. G.; Bas, O.; Dalton, P. D.; De-Juan-Pardo, E. M.; Hutmacher, D. W. Melt Electrospinning Writing of Highly Ordered Large Volume Scaffold Architectures. *Adv. Mater.* **2018**, *30*, 1706570.

(51) Yeo, M.; Kim, G. Micro/Nano-Hierarchical Scaffold Fabricated Using a Cell Electrospinning/3D Printing Process for Co-Culturing Myoblasts and HUVECs to Induce Myoblast Alignment and Differentiation. *Acta Biomater.* **2020**, *107*, 102−114.

(52) Gill, E. L.; Willis, S.; Gerigk, M.; Cohen, P.; Zhang, D.; Li, X.; Huang, Y. Y. S. Fabrication of Designable and Suspended Microfibers via Low-Voltage 3D Micropatterning. *ACS Appl. Mater. Interfaces* **2019**, *11*, 19679−19690.

(53) Yi, B.; Zhang, H.; Yu, Z.; Yuan, H.; Wang, X.; Zhang, Y. Fabrication of High Performance Silk Fibroin Fibers: Via Stable Jet Electrospinning for Potential Use in Anisotropic Tissue Regeneration. *J. Mater. Chem. B* **2018**, *6*, 3934−3945.

(54) Wang, M.; Jin, H.-J.; Kaplan, D. L.; Rutledge, G. C. Mechanical Properties of Electrospun Silk Fibers. *Macromolecules* **2004**, *37*, 6856−6864.

(55) Jayasinghe, S. N.; Irvine, S.; McEwan, J. R. Cell Electrospinning Highly Concentrated Cellular Suspensions Containing Primary Living Organisms into Cell-Bearing Threads and Scaffolds. *Nanomedicine* **2007**, *2*, 555.

(56) Hoogduijn, M. J.; Van Den Beukel, J. C.; Wiersma, L. C. M.; Ijzer, J. Morphology and Size of Stem Cells from Mouse and Whale: Observational Study. *Br. Med. J.* **2013**, *347*, f6833.

(57) Li, L.; Eyckmans, J.; Chen, C. S. Designer Biomaterials for Mechanobiology. *Nat. Mater.* **2017**, *16*, 1164−1168.